

Two-dimensional imaging of dense tissue-simulating turbid media by use of sonoluminescence

Qimin Shen and Lihong V. Wang

An optical imaging technique that is believed to be novel was developed for noninvasive cross-sectional imaging of tissuelike turbid media. By use of a sonoluminescence signal generated internally in the media with a 1-MHz continuous-wave ultrasound, two-dimensional images were produced for objects embedded in turbid media by a raster scan of the media. Multiple objects of different shapes were resolved with this imaging technique. The images showed a high contrast and good spatial resolution. The spatial resolution was limited by the focal size of the ultrasonic focus. © 1999 Optical Society of America

OCIS codes: 110.0110, 110.6960, 110.7050, 110.7170.

1. Introduction

Optical imaging, also known as optical tomography, in strongly scattering media has become an active research field because of its advantages of noninvasion, nonionization, and functional contrast for biomedical diagnosis.^{1,2} Several optical imaging techniques being investigated at present include time-resolved optical imaging, frequency-domain optical imaging, optical coherence tomography, optoacoustic tomography, and ultrasound-modulated optical (acousto-optical) tomography. In these approaches, time-resolved and frequency-domain techniques have achieved a comparable resolution of millimeters. Optical coherence tomography has achieved 10- μm resolution but is limited to a penetration of <2 mm into biological tissues. Optoacoustic tomography and acousto-optical tomography have achieved millimeter resolution and have the potential to image thick biological tissues. The image contrast is based on the difference in optical properties between abnormal and the surrounding normal biological tissues. All these optical approaches use an external light source, usually a laser.

Because biological tissues are optically turbid media, light is diffused quickly in tissues, owing to

strong scattering. Light transmitted through tissues consists of three types: ballistic light, quasi-ballistic light, and diffuse light. Ballistic light travels straight through tissue with no experience of scattering by the tissue and hence carries direct imaging information as does x ray. Quasi-ballistic light experiences minimal scattering in the forward direction and carries some imaging information. Diffuse light follows tortuous paths, carries little direct imaging information, and overshadows ballistic or quasi-ballistic light. For a 5-cm-thick biological tissue with the assumed absorption coefficient $\mu_a = 0.1 \text{ cm}^{-1}$ and reduced scattering coefficient $\mu_s' = 10 \text{ cm}^{-1}$, the ballistic light and quasi-ballistic light, for all practical purposes, do not exist.³ Therefore diffuse light is the only carrier of imaging information for thick biological tissues. All optical tomography for thick biological tissues must overcome the light-scattering problem to obtain optical images.

Ultrasonic generation of light in a medium, known as sonoluminescence (SL), was first discovered in 1934.⁴ The initial observations were multiple-bubble SL. SL has attracted an extraordinary amount of attention in this decade, since single-bubble SL was reported in 1990.⁵⁻¹³ Although the full explanation of SL is still in development, it is well known that light is emitted when tiny bubbles driven by ultrasound collapse. The bubbles start out with a radius of several micrometers and expand to $\sim 50 \mu\text{m}$, owing to a decrease in acoustic pressure in the negative half of a sinusoidal period. After the sound wave reaches the positive half of the period, the situation changes rapidly. The resulting pressure difference leads to a rapid collapse of the bubbles,

The authors are with the Optical Imaging Laboratory, Biomedical Engineering Program, Texas A&M University, College Station, Texas 77843-3120. L. V. Wang's e-mail address is LWang@tamu.edu.

Received 20 April 1998; revised manuscript received 6 July 1998.
0003-6935/99/010246-07\$15.00/0

© 1999 Optical Society of America

accompanied by a broadband emission of light—SL. This process is repeated with each cycle of sound.¹³ The flash time of SL was measured to be in the tens of picoseconds.⁵ Single-bubble SL is so bright that it can be seen by the naked eye even in a lighted room, whereas multi-bubble SL is visible only in a darkened room.¹⁰ The spectrum of SL contains molecular emission bands associated with the liquid, mostly water, in which the SL occurs.¹⁰ A typical spectrum of SL is a broadband emission with peaks near 300–500 nm.¹³ Spectral peaks are also reported at 590, 670, and 770 nm while alkali-metal salts of Na⁺, Li⁺, and K⁺, respectively,⁶ were dissolved in water. From the spectrum of SL in water, the local temperature within the cavities was estimated to be of the order of 5000 K.¹⁰ Researchers have envisaged possible applications of SL in sonofusion, in sonochemistry, and in the building of ultrafast lasers with the ultrafast flash of light in SL, which, with the exception of a laser, is the only means of generating picosecond flashes of light.

We report a comprehensive study of what we believe is a novel application of SL in optical imaging: SL tomography (SLT) of dense turbid media.¹⁴ In SLT minimally scattering ultrasound that generates an internal light source in the media is used to image optically scattering media. SLT contains information not available in the traditional ultrasonography. The major advantages of SLT include (1) high signal-to-noise ratio, owing to the internally generated SL signal; (2) high contrast of imaging; (3) good spatial resolution, which is limited by the ultrasonic focal size; and (4) low cost of equipment. The cost of equipment to generate SL is as low as several hundred U.S. dollars.¹⁵ This paper gives a full account of our investigation, whereas our previous one demonstrated the concept of SLT.¹⁴

2. Methods and Materials

We prepared two types of turbid media: an Intralipid phantom and a polystyrene phantom. We prepared the Intralipid phantom by mixing 8 ml of dominantly scattering Intralipid (Pharmacia Inc., 20%) and 3.25×10^{-8} mol of dominantly absorbing Trypan Blue (Sigma, T5526) in 360 ml of distilled water. The reduced scattering coefficient μ_s' and the absorption coefficient μ_a were 6.15 cm^{-1} and 0.014 cm^{-1} , respectively, at the wavelength of 584 nm, which is the absorption peak of Trypan Blue dye. The reduced scattering coefficient μ_s' is equal to $\mu_s \times (1 - g)$, where μ_s is the scattering coefficient defined as the probability of scattering per unit infinitesimal path length and g is the scattering anisotropy defined as the average cosine of the single-scattering deflection angle. We prepared the polystyrene phantom by mixing 13.4 ml of dominantly scattering polystyrene solution (Interfacial Dynamics Corp., Surfactant-free Polystyrene Latex, 8.1% of solid and $0.91 \pm 0.038\text{-}\mu\text{m}$ in diameter) and 8×10^{-7} mol of the Trypan Blue in 486.6 ml of distilled water. The corresponding μ_s' and μ_a at 584 nm were 7.50 cm^{-1} and

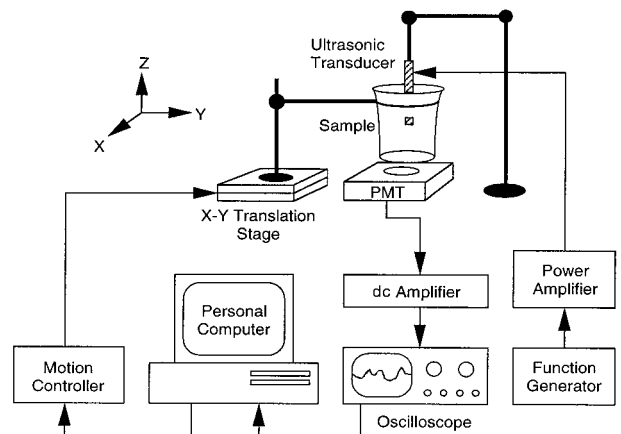


Fig. 1. Schematic diagram of the experimental setup for SL imaging.

0.25 cm^{-1} , respectively. The optical properties of the phantoms were comparable with those of biological tissues.¹⁶ Because the spectrum of the SL is broadband,¹⁷ the optical scattering properties of the scattering media were also given at the wavelength of 400 nm, which corresponds to the spectral peaks of the SL¹⁸ and the maximum-sensitivity spectral range of the optical detector in our experiment. The μ_s' and μ_a of the Intralipid phantom at 400 nm were 8.5 cm^{-1} and 0.002 cm^{-1} , respectively.¹⁹ The μ_s' and μ_a of the polystyrene phantom at 400 nm were 10.8 cm^{-1} and 0.035 cm^{-1} , respectively. The Polystyrene Latex microspheres were used so that the scattering properties of the polystyrene phantom could be calculated with Mie theory.

The turbid solutions were contained sequentially in a 400-ml fused-quartz beaker (Quartz Scientific Inc. Model QBKLO400) and were held on an x - y translation stage (Fig. 1). Objects made of rubber were buried in the phantoms. An ultrasonic transducer (Panametrics Model V314-SU) with a focal length of 3.68 cm, a focal diameter of 0.3 cm, and a focal zone of 3.44 cm transmitted vertically an ultrasonic wave into the scattering medium. The ultrasonic transducer was driven by an amplified 1-MHz sinusoidal signal from a function generator (Stanford Research Systems Model DS345). The amplification was achieved by use of a power amplifier (Mini-Circuits Model TIA-1000-1R8) and a transformer. The height of the ultrasonic transducer was adjusted such that the focal zone of the ultrasonic wave enclosed the buried objects in the vertical direction. The height between the middle plane of the objects and the bottom of the beaker was 4.5 cm. The motorized translation stage, controlled with a personal computer (PC), was able to scan along both the x and the y axes, which formed an x - y plane perpendicular to the ultrasonic axis. The SL signal was detected with a photomultiplier tube (PMT) (Hamamatsu Model R928) beneath the beaker and then was amplified differentially with a low-noise preamplifier (Stanford Research Systems Model SR560). The

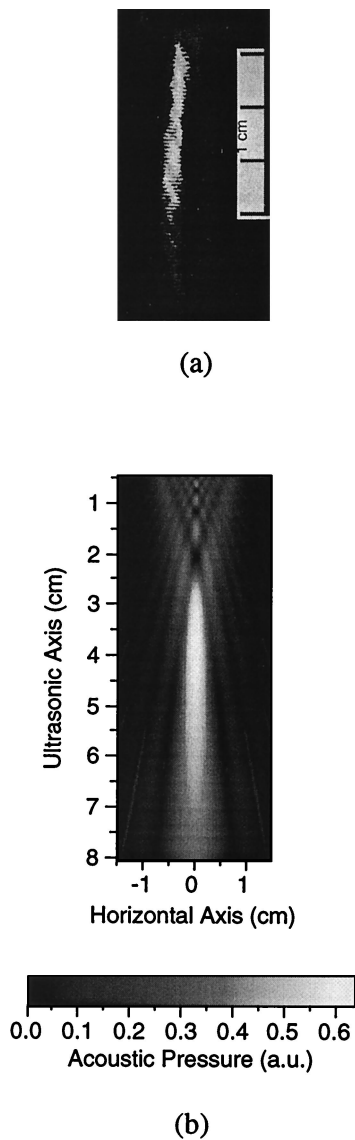


Fig. 2. (a) SL column measured with a CCD camera. (b) Modeled sound column of the ultrasonic transducer.

amplified signal was a dc voltage representing a time-averaged SL intensity with a time constant of ~ 10 ms for the detection system. The amplified signal was recorded with a digital oscilloscope (Tektronix Model TDS 640A) and was subsequently acquired with the PC through a general-purpose interface bus (GPIB) interface (National Instruments, peripheral component interface-GPIB).

During raster scanning of the beaker in the x - y plane with a step size of 1 mm, the PC recorded the dc signals of SL versus the values of x and y . The optical and ultrasonic systems were fixed while the beaker was scanned. Two-dimensional images of the objects buried in the scattering media were plotted with the acquired data.

3. Results and Discussion

Previously, we reported the SL column in a clear solution that was imaged with a CCD camera [Fig.

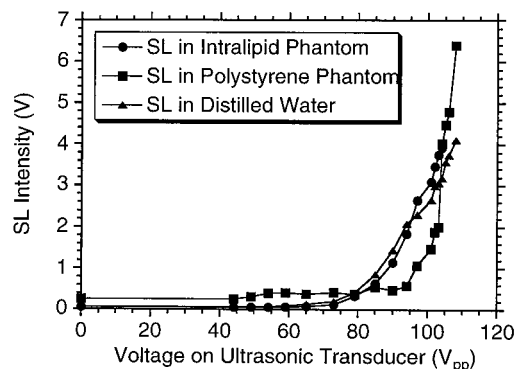


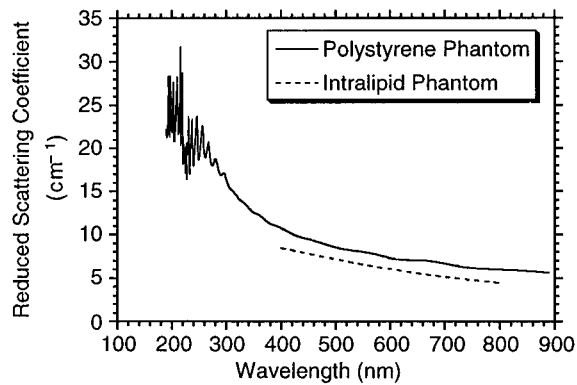
Fig. 3. SL intensity versus the driving voltage on the ultrasonic transducer.

2(a)].¹⁵ We further modeled the distribution of acoustic pressure underneath the ultrasonic transducer, using the following equation:

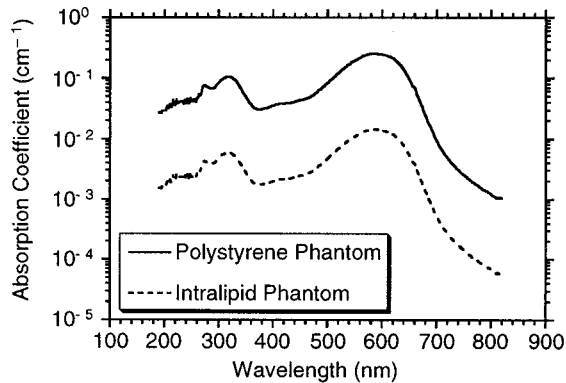
$$p(\mathbf{r}, t) = C \int_s \frac{p(s) \exp[j(\omega t - \phi)]}{d} ds, \quad (1)$$

where $p(\mathbf{r}, t)$ is the pressure as a function of the observation point \mathbf{r} and time t , C is a constant, $p(s)$ is the pressure on the surface of the ultrasonic transducer, ω is the angular frequency of the ultrasonic wave, ϕ is the phase delay from a point on the transducer surface and the point of observation, and d is the distance between a point on the transducer surface and the point of observation. The integration is over the surface of the ultrasonic transducer. The focal length in the calculated sound field matched that specified by the manufacturer [Fig. 2(b)]. The sound column correlated strongly with the SL column.

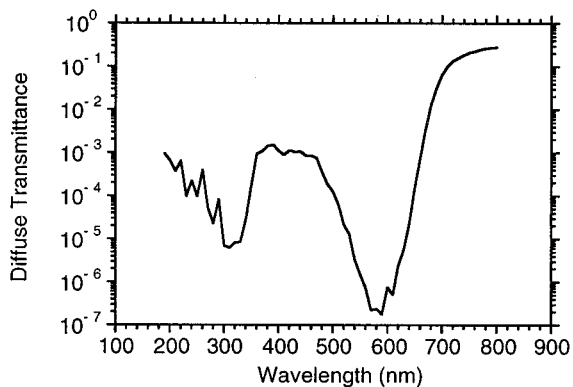
We measured the relation between the SL intensity and the peak-peak voltage applied to the ultrasonic transducer in the two scattering media without buried objects and in distilled water (Fig. 3). The measurements with a hydrophone (Imotec Messtechnik, PVDF-Needlehydrophone) showed that the ultrasonic pressure at the focus was proportional to the peak-peak voltage applied to the transducer. When the peak-peak voltage was 100 V, the peak ultrasonic pressure at the ultrasonic focus was 2.0 bars. This experiment showed clearly that there were thresholds of ultrasonic pressure to generate SL.¹³ When the ultrasonic pressure was increased above the thresholds, the SL intensity increased rapidly with the increasing pressure. Because of the limitation of power on the ultrasonic transducer, we could not measure the upper ultrasonic thresholds, although there must have been some.¹³ The rapid increase of the SL intensity with the acoustic pressure above the thresholds indicated that the SL signal would be a sensitive measure of the local acoustic pressure. It was also observed that generation of SL was not affected by the addition of Intralipid and Trypan Blue but was affected significantly by the addition of polystyrene spheres.



(a)



(b)



(c)

Fig. 4. (a) Reduced scattering spectra for the polystyrene phantom (solid curve) and for the Intralipid phantom (dashed curve). (b) Absorption spectra of the polystyrene phantom (solid curve) and the Intralipid phantom (dashed curve). (c) Diffuse transmittance versus the wavelength for the polystyrene phantom calculated with a Monte Carlo simulation.

Because SL is a broadband emission,¹⁷ the scattering spectra and the absorption spectra were plotted in Fig. 4 for the Intralipid phantom and the polystyrene phantom. In Fig. 4(a) the reduced scattering coefficient of the Intralipid phantom was calculated with Eqs. (12) and (13) in Ref. 18, and the reduced scattering coefficient of the polystyrene phantom was

calculated with Mie theory. The reduced scattering coefficient decreased with increased wavelength. The reduced scattering coefficients of the phantoms were comparable with those of biological tissues.¹⁶ The absorption spectra of the Intralipid phantom and the polystyrene phantom were based on the absorption spectrum of Trypan Blue that was measured with a spectrophotometer [Fig. 4(b)]. The two phantoms contained different amounts of Trypan Blue and hence had different values of absorption coefficient. The peak absorption coefficient was also comparable with that of biological tissues.¹⁴

We calculated the diffuse transmittance of the SL signal as a function of the wavelength with a Monte Carlo simulation [Fig. 4(c)].²⁰ The above optical properties of the polystyrene phantom were used. The phantom in the simulation was assumed to be an 8-cm-thick slab. An isotropic SL point source was placed 3 cm deep in the slab and 5 cm away from the other slab surface that the detector was adjacent to. After experiencing multiple-scattering events, the SL light arrived at the detector. The two valleys in the diffuse transmittance were caused by the absorption peaks of Trypan Blue. Multiplying the transmittance spectrum by the SL spectrum, which is broadband with a peak near 300 nm,¹⁷ we obtained the measured SL signal that had a slightly narrower spectrum peaked at ~ 400 nm, which happened to match the maximum-sensitivity region of the PMT.

After background subtraction by differential amplification, the SL intensity was recorded as a dc voltage. The maximum dc signal was 6.3 V for the polystyrene phantom. The gain of the preamplifier was set to 5×10^4 . The dc voltage across the PMT was -986 V. On the basis of the photocathode radiant sensitivity of 70 mA W^{-1} at the 400-nm wavelength, the total luminescence power received by the 1.92-cm^2 photocathode was estimated to be $1.8 \times 10^{-15} \text{ W}$. On the basis of the calculated diffuse transmittance of the polystyrene phantom near 400 nm [Fig. 4(c)], the SL power at the source was estimated to be greater than 1 pW.

The turbid medium functioned as a filter that modified the spectrum of the SL signal. For biological tissues, the filter would be different from that shown in Fig. 4(c). The SL signal in biological tissues at the short wavelength will be attenuated much more strongly than that at the long wavelength (near the red). The spectral intensity of the SL signal at the source decreases approximately linearly from the peak wavelength to the longer wavelength. The spectral intensity near 600 nm is approximately $1/10$ of the peak spectral intensity.¹⁷ Because light near 600 nm has a much better transmission than light at a shorter wavelength, detection of SL signal in thick biological tissues must rely on light near the 600-nm or longer wavelength.

A rubber cube in the Intralipid phantom was imaged with SLT (Fig. 5). The schematic of the object buried in the Intralipid phantom is shown in Fig. 5(a). The SL intensity as a function of x across the center of the object was plotted in Fig. 5(b), and the

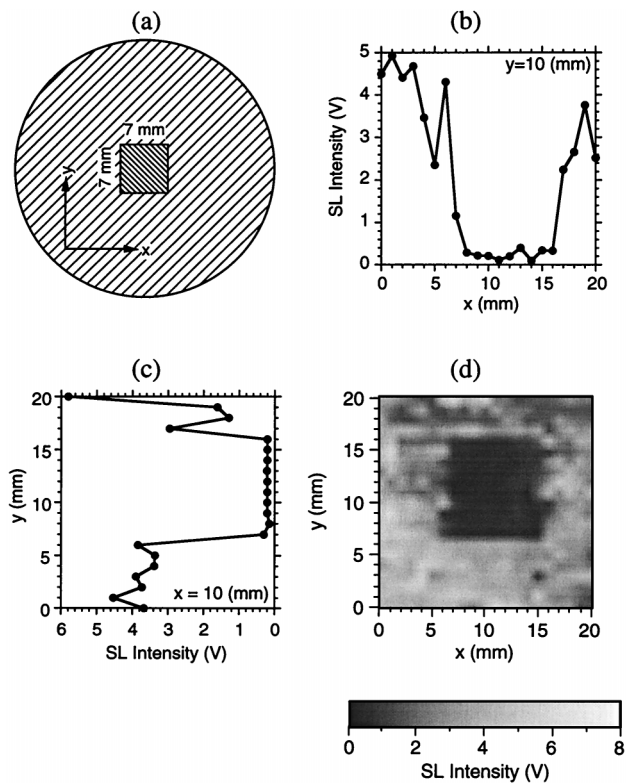


Fig. 5. (a) Schematic diagram of an 8 mm \times 8 mm \times 7 mm cubic object buried in the Intralipid phantom. (b) One-dimensional SL image horizontally across the center of the object (parallel with the x axis at $y = 10$ mm). (c) One-dimensional SL image vertically across the center of the object (parallel with the y axis at $x = 10$ mm). (d) Two-dimensional SL image of the object in the Intralipid phantom.

SL intensity as a function of y across the center of the object was plotted in Fig. 5(c). From these one-dimensional SL images, the spatial resolution of the edges was estimated to be 2–3 mm, and an excellent imaging contrast was observed. A two-dimensional SL image of the cube buried in the Intralipid phantom is shown in Fig. 5(d). A similar two-dimensional SL image of the cube buried in the polystyrene phantom is shown in Fig. 6. The contrast and the spatial resolution were comparable in both two-dimensional SL images.

The contrast of the SL images was based on the difference between the optical and the ultrasonic properties of the objects and those of the surrounding medium. These objects were optically opaque and ultrasonically absorbing. When the object was moved toward the ultrasonic focus, the SL intensity dropped quickly for several reasons. First, the ultrasonic field was reduced below the focus because of the slight acoustic attenuation of the rubber object. Second, the object yielded no SL signal. Third, the SL signal above the object was partially blocked by the object and hence had a more difficult time reaching the PMT.

To observe the spatial resolution for distinguishing multiple objects, we buried two cubic objects in the

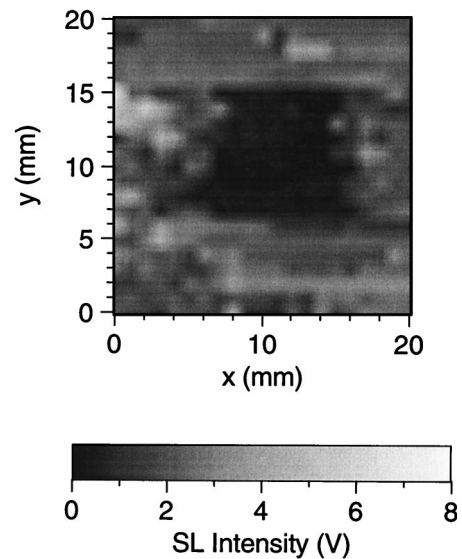


Fig. 6. Two-dimensional SL image of the same object (see Fig. 5) buried in the polystyrene phantom.

Intralipid phantom [Fig. 7(a)]. The distance between the two objects was Δx , which was varied from 1 to 6 mm. One-dimensional SL images across the centers of the two objects were obtained for various distances Δx [Fig. 7(b)]. From these figures we observed the spatial resolution of 2–3 mm, which was similar to that observed in the single-object SL images (Fig. 5). The spatial resolution was limited by the focal size of the ultrasonic transducer, which was 3 mm.

To observe the spatial resolution for revealing the shapes of buried objects, we buried two objects of different shapes in the Intralipid phantom: a square object and a triangular object [Fig. 8(a)]. A two-dimensional SL image of the two objects was acquired [Fig. 8(b)]. The 2-mm separation between the tip of the triangular object and the square object was barely resolved in the SL image. The hypotenuse of the triangular object looked zigzagged because of the 1-mm step size in the raster scanning during the data acquisition. However, both objects were clearly imaged with the correct shapes and sizes.

Although the objects used in this experiment had both optical and ultrasonic contrast relative to the background medium, images of objects can in general be obtained with SLT that is based on several contrast mechanisms. First, when an object has ultrasonic contrast relative to the background, the SL signal originating from the object will differ from that originating from the background medium. As depicted in Fig. 2, the SL generation is affected by the local ultrasonic intensity. Second, when an object has contrast in optical properties, the SL signal from the object will be attenuated differently, because the SL light must propagate through the object. Third, when an object has contrast in ability to generate SL, the SL signal from the object will be different even if the local ultrasonic pressure is the same.

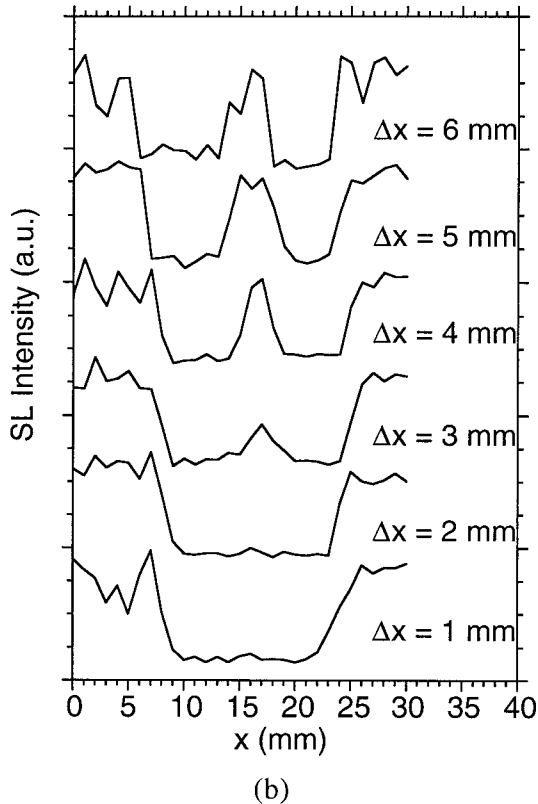
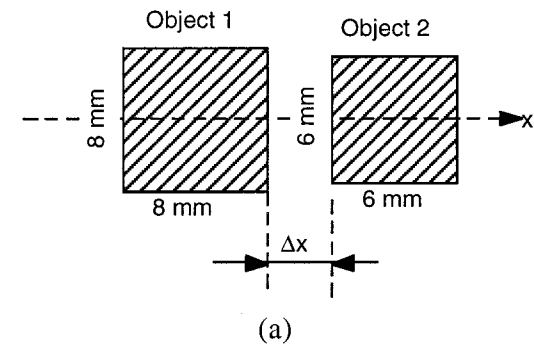


Fig. 7. (a) Schematic diagram of two rubber objects buried in the Intralipid phantom with a separation Δx . (b) One-dimensional SL images of the two objects along the x axis when the separation Δx was varied from 1 to 6 mm.

Using the present ultrasonic system, we obtained a SL column of ~ 3.5 cm in length and ~ 0.3 cm in diameter [Fig. 2(a)].¹⁵ The length of the SL column limits the imaging resolution along the ultrasonic axis. Similarly, the diameter of the SL column determines the imaging resolution on the x - y plane. A more tightly focused ultrasonic transducer can be used to reduce the size of the SL column significantly. When the SL column is reduced to a desired size, one can acquire three-dimensional images of scattering media by scanning in all three directions.

SL light propagates outward in the scattering medium in all directions. We can improve the signal-to-noise ratio of the detection system dramatically by integrating the SL light over a large detection area or

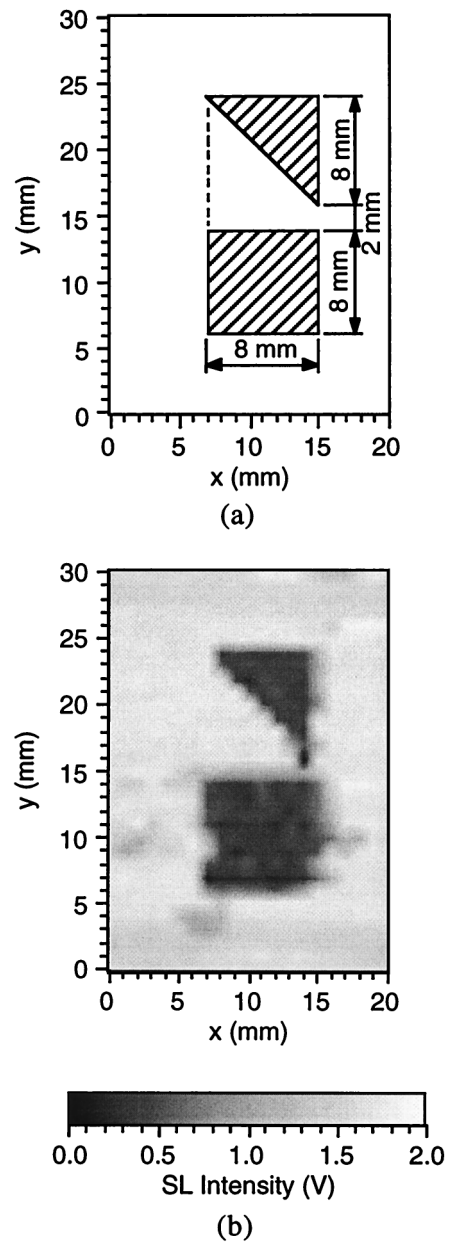


Fig. 8. (a) Schematic diagram of two rubber objects with different shapes buried in the Intralipid phantom. (b) Two-dimensional SL image of the two differently shaped objects buried in the Intralipid phantom.

by a light collection system similar to an integrating sphere. Because all the SL light is useful for imaging, integrating the SL signal would allow an increased imaging depth as well.

Although there are potentially harmful effects caused by cavitation, the threshold of ultrasound intensity that leads to volume lesions is very high. The damage threshold in spatial-peak-temporal-peak power was reported to be 400 and 900 W cm^{-2} at 1 MHz for dog brain tissue and dog thigh muscle, respectively.²¹ The peak pressure in our experiment was ~ 2.0 bars at the ultrasonic focus, corresponding to a spatial-peak-temporal-peak power of 1.3 W

cm⁻², which was two orders of magnitude less than the damage threshold. The peak pressure was also far less than the 23-bar safety limit set by the U.S. Food and Drug Administration, whose standards are usually conservative.²² SLT uses ultrasonic waves to drive preexisting microbubbles between 5 and ~50 μm in size; hence formation of new bubbles with ultrasound is not necessary. The threshold acoustic power to generate SL through preexisting bubbles is much less than that required to form new bubbles. It was also reported that ultrasonic irradiation on cells with acoustic pressures less than a critical value does not cause damage, even if cavitation was observed.²³ Therefore there should be a safety window within which SL can be observed without cause of tissue damage.

4. Conclusions

In conclusion, the sonoluminescence (SL) technique was used to image objects buried in dense tissue-simulating turbid media. Both the spatial resolution and the contrast of the images were quite good. The spatial resolution of 2–3 mm was limited by the ultrasound focal size and might be improved with tightening of the focal size. SLT should be capable of imaging thick biological tissues because of the minimal ultrasonic scattering and the broad SL spectrum. The SLT technique is expected to help with finding applications in biomedicine and other fields that involve scattering media, such as clouds, ocean water, foams, paper, colloids, and dairy products.

Thanks to X. Zhao for her experimental assistance in electronics. This project was sponsored by the National Institutes of Health grants R29 CA68562 and R01 CA71980.

References

1. R. R. Alfano and J. G. Fujimoto, eds., *Advances in Optical Imaging and Photon Migration*, Vol. 2 of OSA Trends in Optics and Photonics Series (Optical Society of America, Washington, D.C., 1996).
2. B. Chance and R. R. Alfano, eds., *Optical Tomography and Spectroscopy of Tissue: Theory, Instrumentation, Model, and Human Studies II*, Proc. SPIE **2979** (1997).
3. L.-H. Wang and S. L. Jacques, "Application of probability of n scatterings of light passing through an idealized tissue slab in breast imaging," in *Advances in Optical Imaging and Photon Migration*, R. R. Alfano, ed., Vol. 21 of OSA Proceedings Series (Optical Society of America, Washington, D.C., 1994), pp. 181–186.
4. H. Frenzel and H. Schultes, "Lumineszenz im ultraschallbeschickten Wasser," *Z. Phys. Chem. Abt. B* **27**, 421–424 (1934).
5. B. P. Barber and S. J. Putterman, "Observation of synchronous picosecond sonoluminescence," *Nature* **352** (London), 318–320 (1991).
6. E. B. Flint and K. S. Suslick, "Sonoluminescence from alkalimetal salt solutions," *J. Phys. Chem.* **95**, 1484–1488 (1991).
7. L. A. Crum and S. Putterman, "Sonoluminescence," *J. Acoust. Soc. Am.* **91**, 517 (1992).
8. C. C. Wu and P. H. Roberts, "Shock-wave propagation in a sonoluminescing gas bubble," *Phys. Rev. Lett.* **70**, 3424–3427 (1993).
9. W. C. Moss, D. B. Clarke, J. W. White, and D. A. Young, "Hydrodynamic simulations of bubble collapse and picosecond sonoluminescence," *Phys. Fluids* **6**, 2979–2985 (1994).
10. L. A. Crum and R. A. Roy, "Sonoluminescence," *Science* **266**, 233–234 (1994).
11. C. Eberlein, "Sonoluminescence as quantum vacuum radiation," *Phys. Rev. Lett.* **76**, 3842–3845 (1996).
12. J. B. Young, T. Schmiedel, and W. Kang, "Sonoluminescence in high magnetic fields," *Phys. Rev. Lett.* **77**, 4816–4819 (1996).
13. B. P. Barber, R. A. Hiller, R. Löfstedt, S. J. Putterman, and K. R. Weninger, "Defining the unknowns of sonoluminescence," *Phys. Rep.* **281**, 65–143 (1997).
14. L.-H. V. Wang and Q. Shen, "Sonoluminescent tomography of strongly scattering media," *Opt. Lett.* **23**, 561–563 (1998).
15. R. A. Hiller and B. P. Barber, "Producing light from a bubble of air," *Sci. Am.* **272**, 96 (1995).
16. W. F. Cheong, S. A. Prahl, and A. J. Welch, "A review of the optical properties of biological tissues," *IEEE J. Quantum Electron.* **26**, 2166–2185 (1990).
17. L. A. Crum, "Sonoluminescence, sonochemistry, and sonophysics," *J. Acoust. Soc. Am.* **95**, 559–562 (1994).
18. Y. T. Didenko, T. V. Gordeychuk, and V. L. Koretz, "The effect of ultrasound power on water sonoluminescence," *J. Sound Vib.* **147**, 409–416 (1991).
19. H. J. van Staveren, C. J. M. Moes, J. van Marie, S. A. Prahl, and M. J. C. van Gemert, "Light scattering in Intralipid-10% in the wavelength range of 400–1100 nm," *Appl. Opt.* **30**, 4507–4514 (1991).
20. L.-H. Wang, S. L. Jacques, and L. Zheng, "MCML—Monte Carlo modeling of light transport in multi-layered tissues," *Comput. Methods Programs Biomed.* **47**, 131–146 (1995).
21. F. J. Fry, N. T. Sanghvi, R. S. Foster, R. Bihrlle, and C. Henige, "Ultrasound and microbubbles: their generation, detection and potential utilization in tissue and organ therapy—experimental," *Ultrasound Med. Biol.* **21**, 1227–1237 (1995).
22. T. A. Whittingham, "The safety of ultrasound," *Imaging* **6**, 33–51 (1994).
23. S. Daniels, T. Kodama, and D. J. Price, "Damage to red blood cells induced by acoustic cavitation," *Ultrasound Med. Biol.* **21**, 105–111 (1995).